Studies of the magnetoelastic inverse Wiedemann effect in pulsed laser deposited cylindrical cobalt films

2004 J. Phys.: Condens. Matter 16 4725

(http://iopscience.iop.org/0953-8984/16/26/007)

INSTITUTE OF PHYSICS PUBLISHING JOURNAL OF PHYSICS: CONDENSED MATTER

J. Phys.: Condens. Matter **16** (2004) 4725–4741 PII: S0953-8984(04)73950-8

Studies of the magnetoelastic inverse Wiedemann effect in pulsed laser deposited cylindrical cobalt films

C Favieres and V Madurga

Laboratorio de Magnetismo, Departamento de Física, Universidad Pública de Navarra, Campus de Arrosadía s/n, Pamplona, E-31006, Spain

E-mail: vmadurga@unavarra.es

Received 27 December 2003
Published 18 June 2004
Online at stacks.iop.org/JPhysCM/16/4725
doi:10.1088/0953-8984/16/26/007

Abstract

Cylindrical soft magnetic Co films, nanostructured with a grain size of 1–2 nm and between ≈1.3 and 90 nm in thickness, were produced by the pulsed laser deposition technique. These films showed a magnetostrictive property. The magnetoelastic inverse Wiedemann effect, or IWE, of longitudinal magnetization as a function of the circular applied magnetic field, M_z–H_ϕ, was measured. The IWE made it possible to explain the magnetization processes according to an initial reversible rotation of the magnetization followed by magnetic wall nucleation and propagation. A magnetization rotation model allowed us to compare the reversible part and the first irreversible magnetization processes corresponding to the IWE. In this way, the values of the helical magnetic anisotropy, K_h, due to the helical stresses, σ_h, generated by an applied torque to the films, were determined. A linear increase of the nucleating magnetic wall field, H_N, with the applied torque, or with σ_h, was observed. In addition, the IWE made it possible to establish the non-dependence of the saturation magnetostriction constant, λ_s, on the sample thickness and to determine the value of this negative isotropic $\lambda_s \approx -4.8 \times 10^{-6}$.

1. Introduction

The pulsed laser deposition technique, PLD, has been successfully applied to the fabrication of thin films, including magnetic and magnetoelastic films [1–12]. A clear understanding of the principles governing the behaviour of these films is of fundamental as well as technological importance. Besides, magnetic Co films can exhibit a soft magnetic behaviour, which makes them suitable for magnetic sensor applications and for devices in micro- and nanoelectronics and micromechanics. Very often, the preparation of amorphous and non-crystalline magnetic films requires the use of various elements to form alloys or compounds, although the fabrication

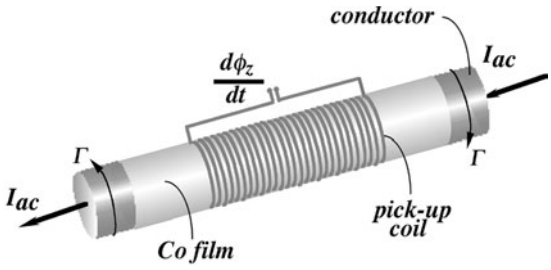

Figure 1. Schematic representation of the inverse Wiedemann effect, IWE, present in our Co cylindrical films. When a helical magnetic anisotropy, K_h, exists in the magnetostrictive PLD Co—i.e., a torque Γ is applied to the wire—and a circular magnetic field H_ϕ—created by an AC electrical current—is applied, an AC voltage can be measured; this voltage being proportional to $d\phi_z/dt$.

of single ferromagnetic elements is possible under certain experimental conditions [4, 7–9, 11–16]. For example, Hiroshima *et al* [4] reported results on the amorphous structure of PLD Co films. We also reported the fabrication of non-crystalline PLD Co films and the soft magnetic properties exhibited by these films [7–9, 11, 12].

In this paper, we show the magnetoelastic properties exhibited by PLD nanostructured Co thin films deposited over metallic wire substrates, therefore having a cylindrical geometry. We explain the magnetization processes as observed by means of the inverse Wiedemann effect, IWE [17]. The IWE is a magnetoelastic effect that has its origin in the coupling between spontaneous magnetization and the helical stresses present in the materials. Any time ferromagnetic materials are subjected to torque, tensile and compressive stresses appear in helical direction, at 45°. The magnetostrictive behaviour of the film leads to magnetoelastic energy, as a function of the angle between the magnetization and the helical stress, to appear. The magnetization will be in one of the two helical directions, depending on the positive or negative sign of the saturation magnetostriction constant. As a result of this helical anisotropy, whenever the sample is subjected to an alternating coaxial circular magnetic field, H_ϕ, a variation of the longitudinal component of the magnetization, dM_z/dt, can be detected, a phenomenon known as the IWE [7, 8, 17–23]. Figure 1 shows a schematic representation of the IWE. A torque, Γ, generates a helical magnetic anisotropy in the magnetostrictive PLD Co; if a circular magnetic field H_ϕ—created by an AC electrical current—is applied, an AC voltage is induced in a pick-up coil, it being proportional to $d\Phi_z/dt$. The ease with which these cylindrical films admit the application of controlled stresses and the simultaneous measurement of the magnetic processes is an advantage of this IWE in comparison with similar studies in planar films.

The knowledge of the magnetization processes exhibited by magnetostrictive amorphous and non-crystalline films and the possibility to characterize these processes through their magnetoelastic behaviour are very interesting from both the theoretical and the applied points of view. From the theoretical point of view, additional information about the magnetic properties of the films is obtained when the non-diagonal term of the magnetic susceptibility tensor, $\chi_{z\phi}$, is measured. It is easier to distinguish between the magnetization processes due to magnetic wall displacements and those due to magnetization rotation, as we shall show in this paper. From an applied point of view, several reasons can be mentioned. On one hand, this induction method presents the advantage that when applying the magnetic field $\boldsymbol{H}$, one does not need a coil to compensate the magnetic flux due to this magnetic field $\boldsymbol{H}$. This is because when measuring the IWE, $\boldsymbol{H}$ is applied in the circular direction and the magnetic flux is picked up and measured in the direction perpendicular to the circular direction, the axial one. It also avoids the existence

of a coil to produce the magnetic field, which is very useful in measurements of the films' magnetic properties. On the other hand, in the IWE of an isotropic sample, the magnetization is measured over the zero level of the applied torque, which means that if there is not an applied torque, there is no effect and there is no signal corresponding to the longitudinal component of the magnetization, M_z. In the IWE, the response of the material is symmetric with respect to the direction of the torque, clockwise or counterclockwise respectively. This is opposite to the conventional magnetization's response of a material under the action of a magnetic field applied in the same direction as the magnetization measurement. That response is different depending on the tensile or compressive stress. The measurement of these magnetoelastic effects is a useful and complementary technique to other techniques for magnetic characterization, such as, for example, vibrating sample magnetometry, VSM, or the superconducting quantum interference device, SQUID. It can also be mentioned that the IWE allows one to determine the helical magnetic anisotropy value and the isotropic magnetostriction constant of the material, K_h and λ_s respectively, which are some of the important parameters of non-crystalline and amorphous materials which do not exhibit crystalline anisotropy. Furthermore, the IWE allows studying the temperature dependence of λ_s that provides deeper information about the mechanism responsible for the magnetoelastic effects and the magnetic anisotropy [20]. In addition, the IWE can be related to the magnetoimpedance phenomenon and it helps to explain the magnetization processes involved in this effect [21].

From this perspective, this work is based on the magnetization processes of PLD non-crystalline cylindrical Co films. We show that the magnetization processes corresponding to the IWE exhibited by these samples were quite different from the IWE loops observed in, for example, Fe whiskers like single crystals [22], amorphous cylindrical CoP electrodeposited multilayers [23], or cylindrical Ni–Fe films [24]. In this paper, we compared the IWE of our amorphous Co films with the same effect exhibited by our CoP amorphous electrodeposited multilayers. The IWE magnetization processes' explanation was complemented by the observation of the magnetic domain wall structure corresponding to the flat samples.

2. Experimental procedures

Cylindrical Co films were prepared by PLD using a stainless-steel chamber (Neocera), which was at a base vacuum pressure of 10^{-6} mbar. The chamber was evacuated using a diaphragm vane pump and a turbomolecular pump. A high pure Co disc (Goodfellow Cambridge Ltd) 99.99%, 20 mm in diameter, was prepared as the target. It was mechanically polished before each ablation process to obtain a surface with a minimal roughness and in order to start all the deposition processes with the same target surface conditions, because it is known that the state of the target relates to the films' properties [4].

We irradiated the polished target for 1 min with the laser beam before each deposition to eliminate possible contaminants from its surface. During PLD, the target was rotated at constant angular speed, 32 rpm. The deposition time was varied between 2 and 90 min. For deposition time higher than 15 min, the time was divided into periods up to 15 min each, in which the laser beam was focused on a different target region. A circular corona corresponding to each period was etched on the target's surface, for a maximum time of 15 min. This made it possible to avoid the effects associated with changes in the morphology of the target surface—e.g. the formation of deep craters [4]—and the decrease in deposition rates during ablation [25]. For this purpose different, but identically prepared, targets were used for deposition times of more than 30 min.

For PLD, a pulsed Nd:YAG laser beam (Quantel's Brilliant), with $\lambda = 1024$ nm, 20 Hz repetition rate, 4 ns pulses, and energy per pulse 220 mJ—just on the target—was introduced

into the chamber through a quartz window. Before each PLD, both sides of the quartz window were cleaned with pure methanol. The energy of the laser was measured using a joule meter (Scientech, mentor MA-10). The laser beam was focused on the target by a lens with a nominal focal length of 600 mm. The area of the laser beam on the target was approximately 13 mm^2. The incidence angle of the laser beam on the target was 45°.

Commercial copper, copper-beryl, tungsten and brass wire 0.5 mm in diameter (Goodfellow Cambridge Ltd) were used as the substrates. In this work we present the results corresponding to the brass wire substrates because of the greater homogeneity of their surfaces and consequently of the deposits. Before the deposition, the wire substrates were cleaned in pure methanol. During the deposition, a home-made system was used to rotate them along their cylindrical symmetry axis at a constant angular speed of 20 rpm, to obtain a homogeneous cylindrical deposit. The substrate wires were placed, in a vertical position, at a distance of 75 mm to the target, and parallel to it. They were at room temperature during PLD. Substrates 80 mm long were used whereas the cylindrical Co deposited film was 40 mm in length. These brass wires were chosen because they exhibit an ample elastic regime under an applied torque. This implies that, as we shall show later, the magnetoelastic behaviour of the Co films grown over them was studied always in the elastic torsion regime of the wire. When measuring the IWE, neither the Co films nor the substrates were plastically deformed, as we deduced from the reversibility of the magnetoelastic and mechanic processes versus the applied torque.

Simultaneously with the deposition of the cylindrical films, plane geometry Co films were deposited on glass and monocrystalline Si (111) substrates, in order to carry out some structural and magnetic characterization. The rate deposition for these planar films was measured as approximately 8 nm min^{-1}.

The IWE measurements were carried out as per the set-up described under [19]. The wire substrate—with the Co film deposited over it—was fixed by two clamps 80 mm apart. The system allows the sample to be subjected to a controlled torque, in both possible directions. Simultaneously, the angular deformation thus produced was measured. The calibration of this system established that $\Gamma/\theta = 3.58 \times 10^{-5}$ N m/deg for our samples.

To measure the IWE, an alternating electrical current flowed through the wire substrate, creating an alternating concentric circular magnetic field, H_ϕ. Due to the thinness of the Co film with respect to the wire diameter—tens of nanometres as compared with 0.5 mm—this magnetic field is considered constant in the entire magnetic sample. A detector coil, 10 mm long, 4000 turns, was situated in the central 10 mm of the Co film and coaxial with it; an electromotive force, emf, was induced in this coil. This emf was generated by the variation of the magnetic induction flux through the cross-section of the cylinder, $d\Phi_z/dt$, due to the variation of the longitudinal component of the magnetization of the Co sample. The emf was then integrated using an electronic flux meter (Walker Magnemetrics, MF-3A), obtaining ϕ_z, where $\phi_z = NS_{\text{film}}B_z$. N is the number of turns of the pick-up coil and $B_z = \mu_0 M_z$ is the magnetization induction corresponding to the longitudinal component of the magnetization. S_{film} is the area of the cross-section of the cylindrical film, $S_{\text{film}} = 2\pi rt$, where r is the radius of the substrate and t is the thickness of the Co film.

As the circular magnetization induction is $B_\phi = \mu_0(H_\phi + M_\phi)$ it was very important to make sure that in each measurement, for each applied torque, the pick-up coil was adequately situated, that is, with its plane strictly perpendicular to the sample. Otherwise, the signal picked up by the coil would be not only dM_z/dt but also the sum of this term plus the contribution due to $(dH_\phi/dt + dM_\phi/dt)$. In this way, after the application of each torque and before each measurement, the detector coil signal was checked as follows. We applied to the film a blocking DC magnetic field ≈200 kA m^{-1}; then we observed the signal picked up by the coil. In this case, no emf in the coil could be observed because the magnetization was fixed

by this blocking field and therefore dM_ϕ/dt and dM_z/dt would be zero. If some signal was observed, it would have to have been produced by dH_ϕ/dt, so the coil must be adequately reoriented until zero signal was observed. The blocking field was then turned off to measure the signal proportional to M_z by integrating $d\phi_z/dt$. This signal proportional to ϕ_z and to M_z was connected to a digital oscilloscope (Tektronik, TDS 3012). So, to monitor the ϕ_z–H_ϕ loops, an AC voltage, proportional to the magnetic field, H_ϕ, was visualized in the horizontal axis of the oscilloscope. This AC voltage was measured across a 400 mΩ manganin resistor connected in series with the brass wire, which constituted the substrate sample. We determined the sign of the magnetostriction constant of these samples by comparing their IWE with the IWE exhibited by a well-known negative magnetostrictive Ni wire (Goodfellow Cambridge Ltd), measured with the same set-up [19].

At this point it should be noted that the experimental system used in this work had some important differences with respect to that described in [8]. In that case the pick-up coil was 40 mm long, with 10 000 turns and a resistance of 735 Ω. In this work the pick-up coil was 10 mm long, with 4000 turns and a resistance of 378 Ω. The change in the number of turns and the corresponding change in the resistance offered better conditions—from our measurements we found them optimum—for the functioning of the flux meter. This fact, together with the new oscilloscope (Tektronik, TDS 3012), instead of the one used in [8] (Tektronik, 2232), allowed us to increase the sensitivity and the accuracy of our IWE measurements. The new 10 mm long pick-up coil explored a reduced region of the cylindrical film, which was probably more homogeneous than that corresponding to the 40 mm long pick-up coil used in the work of [8]. Furthermore, this new 10 mm length allowed us to reorientate the pick-up coil—to eliminate the H_ϕ component in the longitudinal magnetic flux—with greater sensitivity. All these factors gave our system increased sensitivity and higher accuracy. This, in turn, allowed us to obtain new results in detecting and measuring the linear increase of the nucleating magnetic wall field, H_N, with the applied torque, or with σ_h. We had not detected this behaviour with the system used in [8]. For the same reasons, in the present work we were also able to measure the IWE—and to determine the isotropic magnetostriction constant λ_s—in different samples with different thicknesses: from 1.3 to 90 nm. In [8] we measured only one sample thickness.

The relation between the torque applied to the wire and the helical stresses produced is [26]

$$\sigma_h = 2\Gamma r/\pi R^4 \tag{1}$$

where R is the radius of a cylinder subjected to a torque Γ, and σ_h the value of the helical stress inside the cylinder at a distance r from its axis. The value of the helical stress in the Co film, on the surface of the wire—where $r = R$—is $\sigma_h = 2\Gamma/\pi R^3$.

3. Results and discussion

3.1. Structure

The x-ray diffractograms corresponding to the simultaneously deposited planar films showed, in the samples as deposited, the lack of the peaks that are characteristic of crystalline structures. The analysis revealed only a broad peak corresponding to an amorphous structure [7, 9]. These results are in agreement with the work of Hiroshima *et al* [4] who reported the preparation of amorphous PLD Co.

The electron diffraction analyses corresponding to the as-deposited films, see figure 2, revealed broad diffused rings of amorphous-like structure. Microphotographs obtained by high resolution transmission electron microscopy, HRTEM, (PHILIPS CM 200 FEG) showed a structure made up of an assembly of nanograins whose size was $\leqslant$1–2 nm. This absence

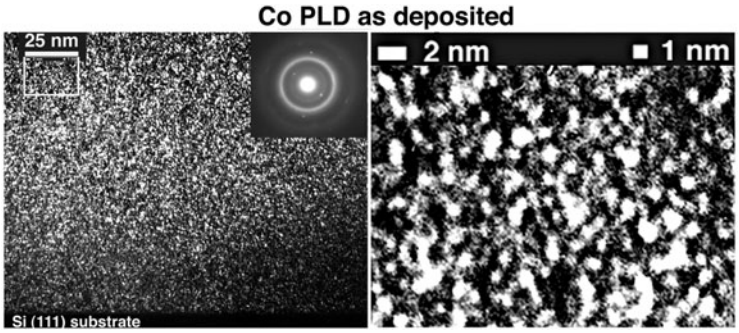

Figure 2. High resolution transmission electron microscopy, HRTEM, results: microphotographs of bright field image showed a structure formed by an assembly of nanograins whose size was $\leqslant$1–2 nm. The electron diffraction analyses corresponding to the films as deposited revealed broad diffused rings of amorphous-like structure, shown in the left-hand part of the figure. The right of the figure is a digital magnification of a portion of this microphotograph.

of long-range crystalline order avoids the existence of crystalline magnetic anisotropy so that only shape anisotropy and stress—magnetoelastic—anisotropy will be present in the films. In the case of Co PLD films, the absence of crystalline magnetic anisotropy gave the amorphous films a soft magnetic property: a low coercive field and a low anisotropy field [7–9, 11]. These two sources of the magnetic anisotropy and their dependence on the films' thickness could give these films peculiar properties with respect to their magnetic domain wall type and their dependence on the film thickness.

3.2. Magnetism

We recorded the soft magnetic behaviour, characteristic of an amorphous magnetic material, exhibited by these simultaneously deposited geometrically flat Co films, [7–9, 11]. The coercive field was of the order of 50–80 A m^{-1}, and a close to bistable magnetic behaviour was observed. The local magnetic field anisotropy was of the order of 950–1200 A m^{-1}.

The magnetic domain structure corresponding to planar Co films has been published previously. In those works we observed the magnetic wall nucleation and later magnetic wall propagation [8, 9, 12, 27], which were related to the irreversible magnetization processes corresponding to the IWE as observed in our cylindrical Co films.

3.3. Magnetoelasticity

Figure 3 shows a representative dependence of the IWE loops on the applied magnetic field, H_ϕ. This behaviour was common for all the cylindrical Co samples studied in this work. We shall describe the loops corresponding to a film, $\approx$63 nm thick, subjected to a magnetic field H_ϕ ($\nu = 23$ Hz) gradually increasing from zero to 2.0 kA m^{-1} and simultaneously to a torque of $\Gamma = 7.2 \times 10^{-4}$ N m. The thickness of the film was measured taking into account the fact [27] that all these loops were saturated with respect to the applied torque, Γ, which meant that for this Γ and for the maximum magnetic field, the amplitude of the loops was maximum. In these cases one can assume that for this Γ and for zero field all the magnetization was settled in the 45° helix, and, consequently, M_{zr} was maximum: $M_{zr} = \cos(45)M_s = 0.71M_s$. The sensitivity of our system allowed us to detect magnetic flux values of $\phi_{min} \approx 3.8 \times 10^{-8}$ Wb. $\phi_{maximum} = \mu_0 M_s NS$, the saturation magnetization of our Co films being $\mu_0 M_s = 1$ T [9].

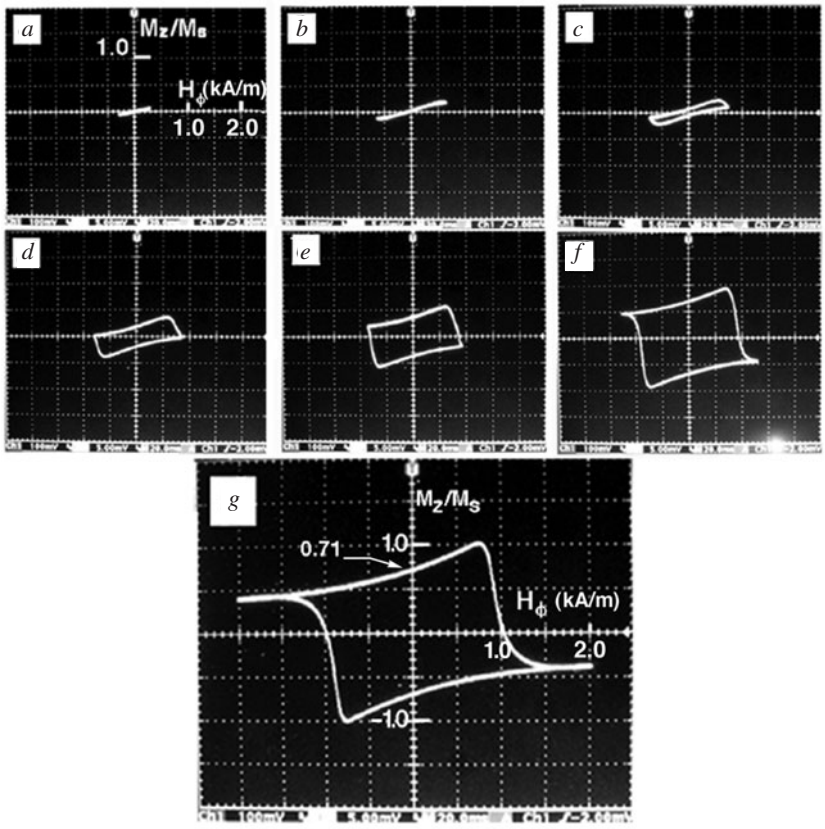

Figure 3. Dependence of the IWE loops, M_z–H_ϕ, on an increasing applied circular magnetic field, H_ϕ, from zero to 2.0 kA m^{-1}. The film was simultaneously subjected to a torque of 7.2×10^{-4} N m.

Using this last magnetization value and the measured ϕ_z we deduced the value of the cross-section of the film, S, from which we could in turn deduce the film's thickness.

Throughout this work, the torque, Γ, in the clockwise direction was called positive torque, and that applied in the counterclockwise direction was called negative torque. The IWE loops of figure 3 are described as follows. For $H_{\phi\text{maximum}} \leqslant 600$ A m^{-1}—figures 3(a) and (b)—, the magnetization process was reversible and for a H_ϕ positive corresponded to a positive value of M_z. The irreversible magnetization processes began for field $\approx$700 A m^{-1}—figure 3(c)—at which point a hysteretic loop appeared. For a maximum applied field $H_{\phi\text{maximum}} \approx$ 900 A m^{-1}—figure 3(d)—M_z was zero and from this point, for a maximum positive H_ϕ the corresponding M_z was negative, figures 3(e)–(g). For $H_{\phi\text{maximum}} > 1500$ A m^{-1}—figures 3(f) and (g)—M_z corresponding to the maximum H_ϕ decreased for sufficiently large H_ϕ. The magnetization transferred to the applied circular magnetic field direction, and therefore the longitudinal component of the magnetization decreased. There are three important features which describe the hysteresis loops: (1) a so-called 'nucleation magnetic field' for which the first irreversible processes took place, H_N. This field was associated with magnetic wall nucleation; (2) in figure 3(g) the value of the remanence was $M_\text{zr} = 0.71M_\text{s}$, and (3) in figure 3(g) the value of the maximum $M_z/M_\text{s} = 1$. The value of $M_\text{zr} = 0.71M_\text{s}$ indicated that this applied Γ was large enough to settle, for zero field, all the magnetization in the 45° helix and, consequently, M_zr was $M_\text{zr} = \cos 45°M_\text{s} = 0.71M_\text{s}$, as pointed out above.

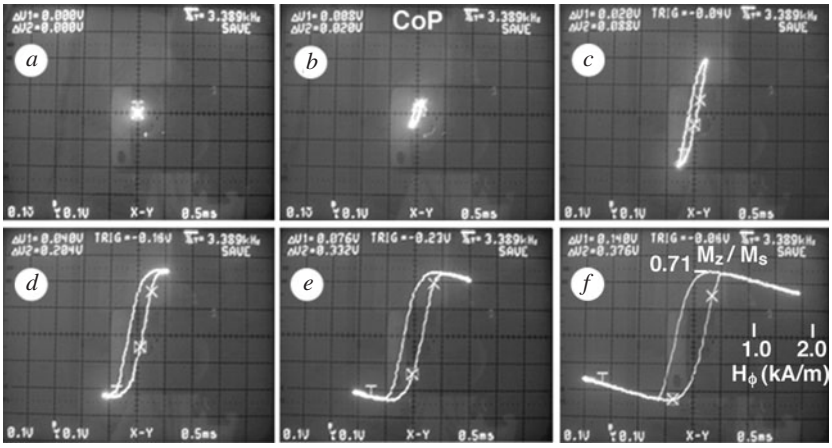

Figure 4. IWE loops corresponding to a CoP cylindrical multilayer electrodeposited onto a copper wire. The sample was simultaneously subjected to torsion big enough to saturate the effect. Vertical and horizontal scales are the same in all six photos.

To compare the IWE loops of our Co PLD films with those irreversible processes governed exclusively by magnetic wall displacements, in figure 4 we have shown the IWE loops corresponding to a $Co_{80}P_{20}/Co_{78}P_{22}$ cylindrical multilayer—≈4 μm thick—electrodeposited onto a copper wire. A study of the magnetic properties of these CoP multilayers has been published elsewhere [23]. The IWE measurements were carried out as described for our Co PLD films, with the same set-up [19]. These six photographs show the six IWE loops as a function of the amplitude of the magnetic field H_ϕ, the sample being simultaneously subjected to an ample torsion that saturated the effect. The scale represented in figure 4(f) is the same for all six photos. First of all, M_z was always positive for H_ϕ positive. The irreversible processes took place at the beginning and for $H_{\phi\text{maximum}} < 500$ A m^{-1}, see figures 4(a)–(d), they were probably irreversible magnetic wall movements; increasing H_ϕ increased the IWE maximum signal. Increasing $H_{\phi\text{maximum}}$ above ≈500 A m^{-1} caused the magnetization to rotate reversibly towards the circular direction, as seen in figures 4(e) and (f), while M_z decreased but remained positive.

To explain the IWE magnetization processes let us consider a uniaxial helical magnetic anisotropy whose easy axis forms a 45° angle with the longitudinal axis of the sample. Figure 5 schematically represents two possible magnetization processes and the corresponding hysteresis loops and switching magnetization curves, M_z–H_ϕ. In figure 5(I), for the initial magnetization processes irreversible magnetic wall displacements are assumed, followed by reversible magnetization rotation to reach saturation. In figure 5(II), reversible magnetization rotation followed by magnetic wall nucleation and propagation is taken into account. In case (I) when an AC H_ϕ is applied, for example in the positive direction, figure 5(I)A, the magnetic domain in which the magnetization has its circular component in the same direction as H_ϕ increases due to the irreversible wall displacement, and a positive net component of the longitudinal magnetization M_z is generated. Increasing positive H_ϕ causes M_z to increase, figure 5(I)B, until, for a value of H_ϕ, the maximum value of M_z is reached, figure 5(I)C. This maximum occurs when all the magnetization is in one of the two 45° helices and $M_z \approx 0.71 M_s$. When this happens, almost all the magnetic walls have disappeared, the sample having become a single domain. At this point an increase of the positive H_ϕ produces reversible magnetization rotation from the helical direction to the direction of the circular magnetic field, figure 5(I)D

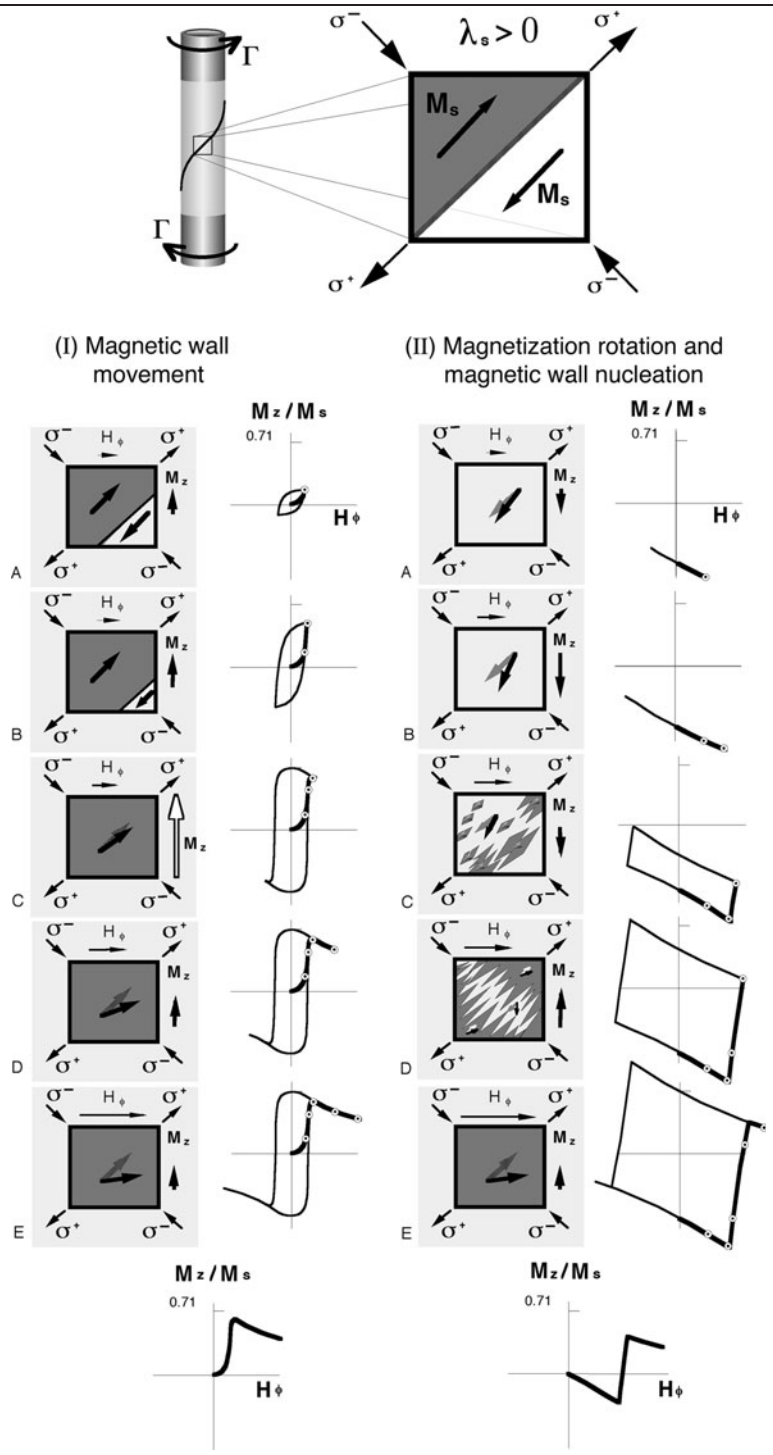

Figure 5. Schematic representation of two possible magnetization processes due to (I) irreversible magnetic wall displacement followed by reversible rotation, and (II) reversible magnetization rotation, magnetic wall nucleation and propagation, and reversible rotation. The corresponding hysteresis loops and magnetization curves are plotted. The magnetization processes shown in figures 3 and 4 are well explained by the processes described in (I) and in (II), respectively.

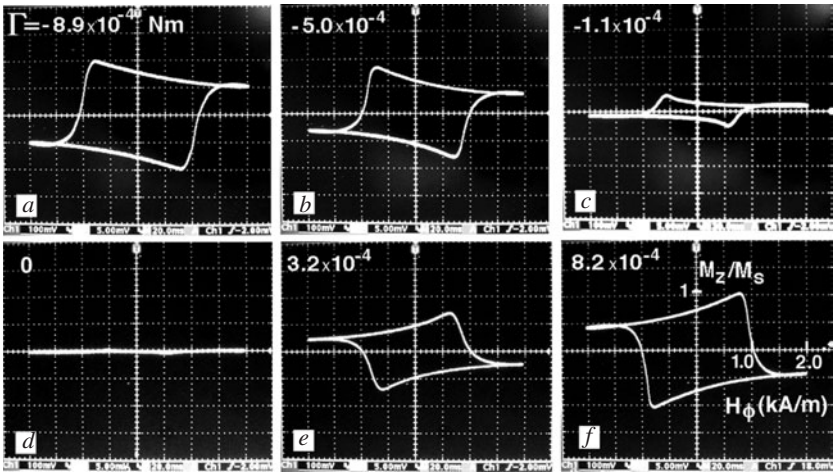

Figure 6. IWE loops dependent on the applied torque, Γ. These were obtained when $H_{\phi\max} = 2.0$ kA m^{-1} was applied simultaneously to Γ. In this sequence Γ varied from -8.9×10^{-4} N m to $+8.2 \times 10^{-4}$ N m. These loops correspond to a PLD Co sample 63 nm thick.

and E. M_z decreases until no M_z can be detected, and all the magnetization is in the circular direction. In these figures one can see the hysteresis loops and the switching magnetization curves corresponding to this process. In the switching curve, M_z is always positive for positive H_ϕ. As can be seen, the magnetization processes corresponding to the IWE $Co_{80}P_{20}/Co_{78}P_{22}$ cylindrical multilayer shown in figure 4 are well explained by a magnetization process similar to those shown in figure 5(I).

Now let us turn our attention to the representation of the magnetization processes schematically shown in figure 5(II). When a low positive circular magnetic field H_ϕ is applied, figure 5(II)A, there is reversible magnetization rotation, the net longitudinal component of the magnetization being other than zero and negative. For a positive increase of the field intensity, the negative value of M_z increases, figure 5(II)B. When the applied field increases above a critical value, magnetic walls nucleate due to irreversible rotations of the magnetization in some regions of the sample, figure 5(II)C. This magnetic wall nucleating process is complemented by our observation in planar films of these new magnetic walls by the Bitter technique; see [8, 9, 27]. For a positive H_ϕ, M_z is still negative, but its value decreases. When H_ϕ is increased more magnetic walls are nucleated and propagate, and at a certain positive value of the field, M_z becomes positive, figure 5(II)D. Finally, reversible magnetization rotation again takes place, until no M_z can be detected because all the magnetization has rotated to the circular direction, figure 5(II)E. The corresponding IWE hysteresis loops and the switching curves represented in this figure are quite similar to those observed in our PLD Co films.

Figure 6 shows a set of IWE loops for one of our cylindrical Co PLD film, as a function of the applied torque, Γ, maintaining the amplitude of the applied magnetic field $H_{\phi\max} = 2.0$ kA m^{-1}($\nu = 23$ Hz). In this sequence Γ varied from -8.9×10^{-4} to $+8.2 \times 10^{-4}$ N m. These photographs correspond to a cylindrical PLD Co sample 63 nm thick. Positive hysteresis loops were generated for negative Γ because of the negative sign of the magnetostriction constant. When the negative Γ decreased, the loop decreased its amplitude; see figure 6 (from (a) to (d)). We note again that for zero Γ there was no magnetic signal in the IWE, figure 6(d). When Γ was applied in the positive direction, figures 6(e) and (f), an IWE loop with the opposite, negative, sign was generated. If this positive Γ

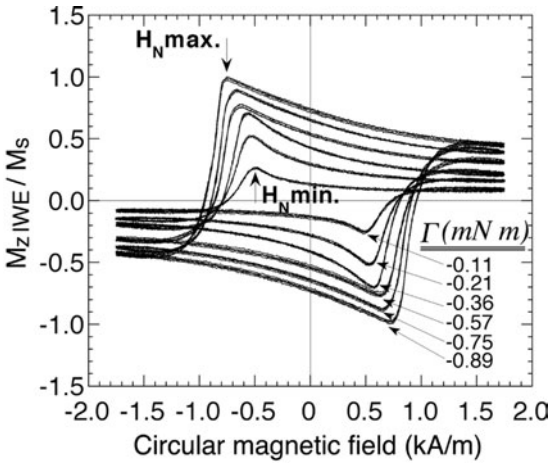

Figure 7. IWE loops corresponding to a single film subjected to different applied torque Γ. The values of the torque are displayed. Note the increase of the nucleation magnetic field, H_N, when Γ increases.

increased, the IWE loop increased its amplitude in the same way as in the case of the positive loops. Qualitatively, these IWE hysteresis loops were interpreted by considering that for zero Γ the tensile and compressive helices were equally filled, and, consequently, due to longitudinal compensation of the magnetization, there was no IWE signal. If a negative Γ was applied to the film, its magnetization was requested by the compressive helix (due to the negative nature of the magnetostriction constant). Part of the magnetization transferred to the compressive helix, and an IWE positive hysteresis loop appeared. When Γ gradually increased, the IWE signal increased in the same proportion until a maximum was reached at which the total magnetization was in the compressive helix. If the torque applied to the sample was eliminated, the IWE took reversibly the zero value. In this situation, if the sample was twisted in the opposite direction, the positive one, the magnetization transferred to the opposite helix than before, and loops with a negative sign were generated. It is worth noting the symmetry of the IWE with respect to the applied torque in both directions, clockwise and counterclockwise. This advantage is not present in geometrically flat samples for conventional magnetic measurements; there is no similar symmetry when tensile or compressive stresses are applied to the samples. To show the influence of the torque applied to the samples on their IWE, in figure 7 we have represented six IWE hysteresis loops for the same sample subjected to different applied torques. The change in the nucleating magnetic field, H_N, produced by the applied torque can be clearly observed, and we will use this fact later.

For applied torque greater than $\approx 8.5 \times 10^{-4}$ N m—both positive and negative—the IWE loop amplitude did not increase. The IWE versus the applied torque is then saturated. This saturating behaviour is produced exclusively by a magnetic effect: no plastic or elastic effects are present. In fact, as can be seen in figure 8(a), there is a linear relation between the applied torque, Γ, and the angular deformation produced by this torque. Figure 8(a) shows this relation for a film 63 nm thick. This behaviour was the same for all the films. In contrast, there was a saturation of the magnetoelastic behaviour exhibited by our films, as shown in figure 8(b). The value of M_{zr} was maximum when the applied torque was $\approx 8.5 \times 10^{-4}$ N m ($\sigma_h = 34$ MPa) which means that this helical stress is sufficient to arrange the magnetization in the 45° helix.

To explore the origin of the irreversible magnetization processes we took measurements of the IWE at different frequencies of the circular magnetic field, the sample being subjected

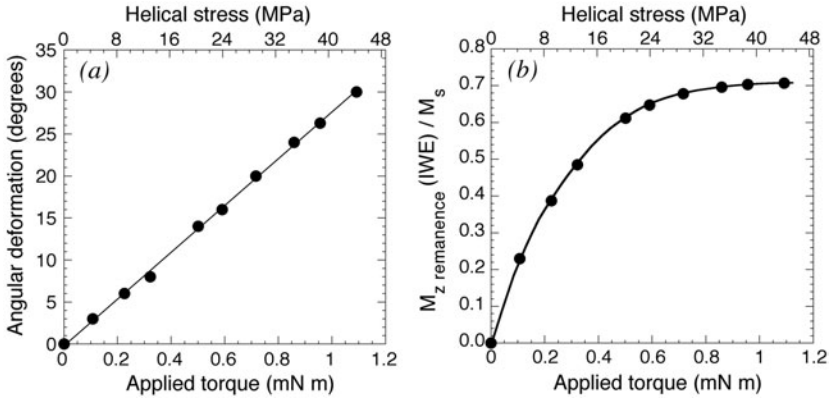

Figure 8. (a) Dependence of the angular deformation of the samples on the applied torque: note the linear relation between them. (b) Dependence of the IWE remanent longitudinal magnetization on the applied torque: note the saturation of the IWE. The curves help to guide the eye.

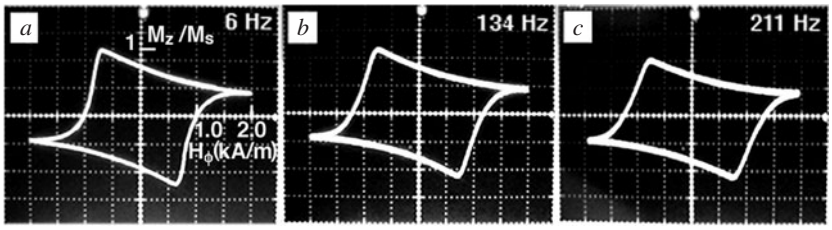

Figure 9. IWE loops measured at different frequencies of the alternating circular magnetic field. $H_{\phi\,\max} = 2.0$ kA m^{-1}. In all cases the film was subjected to $\Gamma = 8.9 \times 10^{-4}$ N m. These loops correspond to a PLD Co sample 79 nm thick.

to the same saturating torque. As is shown in figure 9, there was a clear influence of the frequency on the irreversible part of the magnetization processes. In any case, for very low frequencies, these irreversible processes did not appear as strictly vertical lines in the hysteresis loop, as would correspond to a single irreversible rotation of the magnetization. On the basis of these experimental results, we associated the irreversible rotation of the magnetization with the nucleation of several magnetic walls. After this, more irreversible processes were produced by the magnetic wall propagation.

Another noteworthy feature is that there were no significant changes in the values of the nucleation magnetic field in relation to the frequency of the exciting magnetic field. Neither was any change observed in the reversible magnetization rotation part of the IWE loops in this range of frequency.

In order to explain the magnetic behaviour of our cylindrical samples according to their IWE loops, we shall consider a magnetization rotation model. Figure 10(e) represents a single magnetic domain with a uniaxial magnetic anisotropy, K, whose direction forms an angle θ_0 with the longitudinal axis (z-axis) of the sample. When a magnetic field H_ϕ was applied, the magnetization, M_s, rotated towards the circular direction until its equilibrium position lay at the angle θ against the longitudinal axis. This equilibrium position corresponded to the minimum free energy density. Considering the terms due to Zeeman energy density and anisotropy energy density, the expression for this free energy density was

$$E = E(H_\phi) + E_{\text{anisotropy}} = -\mu_0 M_s H_\phi \cos(\pi/2 - \theta) + K \sin^2(\theta - \theta_0). \qquad (2)$$

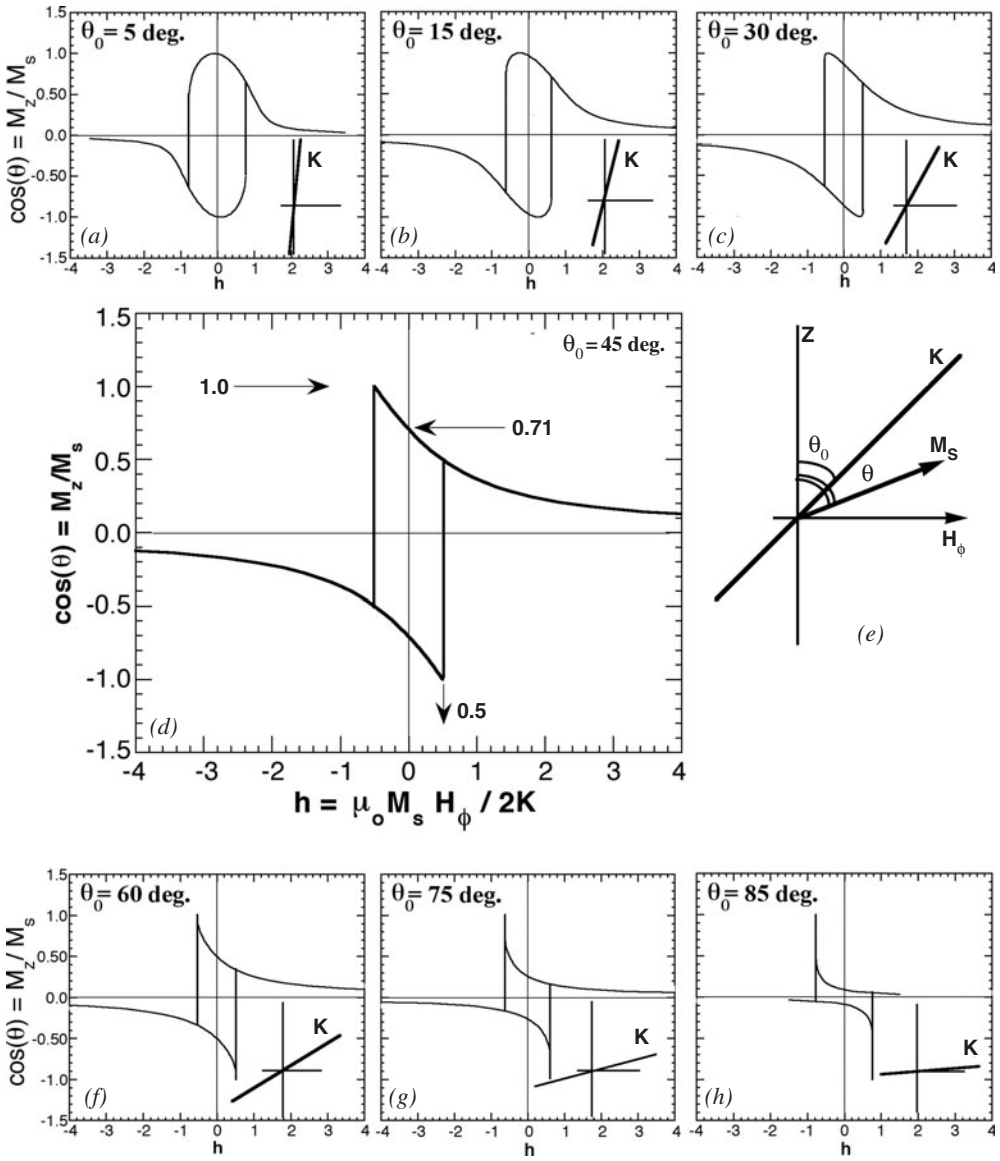

Figure 10. Schematic representation of a magnetization rotation process corresponding to a single magnetic domain with a uniaxial magnetic anisotropy, K. The direction of K forms an angle θ_0 with the longitudinal axis (z-axis) of the sample (e). When a magnetic field H_ϕ was applied, the magnetization M_s rotated towards the circular direction until its equilibrium position lay at the angle θ against the longitudinal axis. (a)–(d), (f)–(h): for different directions of K, hence different θ_0, it was possible to calculate the corresponding IWE loops.

Minimizing equation (2) with respect to the angle θ, we obtained

$$\mu_0 M_s H_\phi / K = \sin(2\theta - 2\theta_0)/\cos\theta. \tag{3}$$

We defined the reduced magnetic field as $h = \mu_0 M_s H_\phi / 2K$, and therefore equation (3) was rewritten:

$$h = \sin(2\theta - 2\theta_0)/2\cos\theta. \tag{4}$$

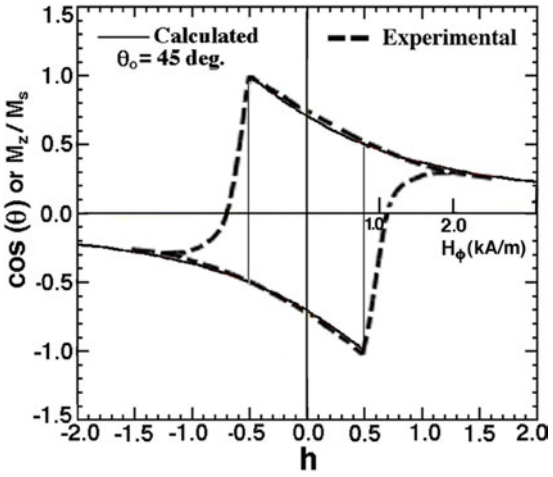

Figure 11. Adjustment of the reversible part and the first irreversible magnetization processes for one of our IWE loops, according to a magnetization rotation model, with an easy direction for the magnetization at 45°, $K = K_{\mathrm{h}}$. From this correspondence we determined the value of $H_\phi = H_{\mathrm{N}} = 830$ kA m^{-1} when $h = 0.5$, and then $K_{\mathrm{h}} = \mu_0 M_{\mathrm{s}} H_\phi / 2h \approx 830$ J m^{-3}.

From these equations, it was possible to calculate the IWE loops corresponding to different directions of K, i.e. to different θ_0; see figures 10(a)–(d), (f)–(h). All our experimental IWE loops adjusted best and *exclusively* with the calculated hysteresis loop corresponding to $\theta_0 = 45°$, as we shall confirm. This means that the direction of K was the 45° helix, $K = K_{\mathrm{h}}$. It is important to note that *only* for this value, $\theta_0 = 45°$, M_{zr} is equal to $0.71 M_{\mathrm{s}}$. In fact, $M_{\mathrm{zr}}/M_{\mathrm{s}} = \cos\theta_0$, and this dependence of the remanence on the direction of the anisotropy allowed us to select this value of 45° for all our IWE hysteresis loops. Furthermore, as it is possible to see in figure 10, the relation between M_{zmax} and M_{zr} is $M_{\mathrm{zmax}}/M_{\mathrm{zr}} = 1/0.71$ only in the case of $\theta_0 = 45°$.

Once the direction of $\theta_0 = 45°$ had been selected to describe the behaviour of all the samples according to all our IWE hysteresis loops, we adjusted one of these loops. We used the calculated values from a magnetization process due exclusively to magnetization rotation with an easy direction for the magnetization at 45°. Figure 11 shows an adjustment for a film 63 nm thick, where it can be seen that the data and the calculated values correspond. Since in the calculated loops irreversibility was produced at $h = 0.5$, we compared this value with the beginning of irreversibility in the hysteresis loops of our samples. Once this was done, we compared the amplitude of the calculated loop with the amplitude of the experimental one. It was found that the calculated loop corresponded perfectly with the two reversible regions of the experimental one. The deduced value of H_ϕ—from the correspondence—when $h = 0.5$, and the knowledge of $\mu_0 M_{\mathrm{s}} = 1$ T, made it possible to determine the value of the helical magnetic anisotropy, $K_{\mathrm{h}} = \mu_0 M_{\mathrm{s}} H_\phi / 2h$. In the case shown in figure 11, $h = 0.5$ corresponded to $H_\phi = H_{\mathrm{N}} = 830$ A m^{-1}, and therefore $K_{\mathrm{h}} \approx 830$ J m^{-3}. This K_{h} value, of course, also corresponded to the reversible parts of the IWE loop. In the theoretical loop, the irreversible jump of the magnetization was strictly vertical because it was due to coherent magnetization rotation and no magnetic wall nucleation—incoherent magnetization rotation—was considered.

To make a more detailed study of the dependence of the IWE on the torque Γ which was already described, in figure 7 we show the IWE loops corresponding to a single film subjected

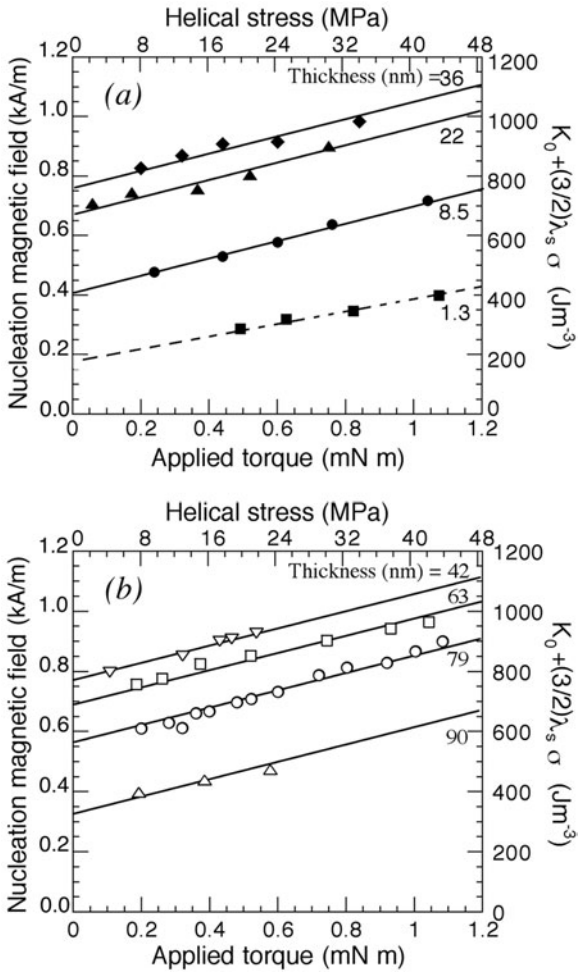

Figure 12. Evolution of the nucleation magnetic field according to the applied torque for different films. The films have different thicknesses, as indicated in the plan. All the continuous straight lines drawn in (a) and (b) have the same slope and correspond to the value of $\lambda_s \approx -4.8 \times 10^{-6}$. (a) Behaviour of four films from 1.3 to 36 nm thick: note that the values of H_N for $\Gamma = 0$ increases with thickness; (b) film thickness varying from 42 to 90 nm: in these cases H_N for $\Gamma = 0$ decreases with thickness.

to different torque, Γ. A clear increase of the nucleation magnetic field H_N can be seen when the applied torque Γ is increased. This behaviour was common for all our films, as shown in figure 12. Figures 12(a) and (b) show that this increase of $H_{N,}$ and therefore of $K_{h,}$ with the applied torque for different samples is a linear increase in all cases. It is important to note that the increase of H_N with Γ is very similar, and is linear for all the samples. In part (a) of figure 12, we plotted the behaviour of four films with different thicknesses, varying from 1.3 to 36 nm. The values of the corresponding H_N—for $\Gamma = 0$—increase with thickness; in contrast, part (b) of the figure demonstrates that for greater thicknesses, from 42 to 90 nm, the corresponding H_N—for $\Gamma = 0$—decreases with thickness. Since the stresses generated in the material by the torque were linear with Γ, the magnetoelastic anisotropy can be expressed as

$$K_h = K_0 + (3/2)\lambda_s\sigma_h. \tag{5}$$

This expression agreed with our experimental results shown in figure 12 and was also used in [28]. Using a magnetic wall nucleation model, the coercivity can be ascribed to this anisotropy, and the nucleation of domain walls led to a linear increase with the anisotropy [28]. In our case, one can consider K_0 as an equivalent anisotropy corresponding to the nucleation field, H_N ($\Gamma = 0$), and thus zero σ_h, $H_{N,\Gamma=0}$.

As mentioned above, in figure 12 it can be seen that the linear dependence of this H_N with Γ, or with σ_h, is similar for all the films. In fact, all the straight lines drawn in figures 12(a) and (b) had the same inclination which corresponded to the same value of $\lambda_s \approx -4.8 \times 10^{-6}$, showing the proper adjustment of all our experimental results. Only the data corresponding to the thinnest sample, 1.3 nm,—dotted line—do not correspond to this λ_s value. This could be due to the small signal of the IWE corresponding to the lowest values of the applied torque. The value of λ_s obtained in this work differs from the value found in [8] because in that case we did not detect the change in the nucleating magnetic field $H_N(\Gamma)$ produced by the applied torque. On that occasion we assigned the helical anisotropy K_h the value due to the helical stress, $\sigma_{h,sat}$, which produced the saturation of the IWE, $K_h = (3/2)\lambda_s\sigma_{h,sat}$. In the present work, due to the higher sensitivity and accuracy of our experimental system, the value of λ_s has been deduced from the derivative of the nucleating magnetic field, $\partial H_N(\sigma_{h,})/\partial\sigma_h$, with respect to the applied helical stress or from the expression, $K_h = K_0 + (3/2)\lambda_s\sigma_h$, according to our experimental results.

The dependence of $H_{N,\Gamma=0}$ on the thickness of the cylindrical films could be associated with the change in the nature of the magnetic walls. The absence of magnetocrystalline anisotropy—whose value could be independent of the film's thickness—in these amorphous films could produce new results with respect to those obtained previously. The residual stresses in the films—not constant and not homogeneous with the film's thickness—and the films' shape could be the source of their anisotropy. This type of heterogeneous anisotropy could produce a different behaviour—with respect to the crystalline one—with typical thickness figures for transition from one to another type of magnetic domain wall. At this point a more specific study must be carried out to obtain more experimental results about this change in the nucleating magnetic field with the film's thickness—derived from the magnetoelastic studies of this work.

4. Conclusions

Cylindrical soft magnetic Co films, between ≈1.3 and 90 nm in thickness, and 1–2 nm grain size, were produced by PLD. These films were magnetostrictive. The magnetoelastic inverse Wiedemann effect made it possible to explain the magnetization processes according to an initial reversible magnetization rotation followed by magnetic wall nucleation and propagation. A final reversible magnetization rotation completed the magnetization processes. By adjusting the IWE according to this model the helical magnetic anisotropy values, K_h, were found. K_h was generated by the helical stresses, σ_h, produced by the torque applied to the films. A linear increase of the nucleation magnetic fields, H_N—which produces the first irreversible magnetization processes—was observed when the applied torque increased. We determined the value of the negative isotropic saturation magnetostriction constant, $\lambda_s \approx -4.8\times10^{-6}$, from this linear dependence behaviour. We also confirmed this same quantitative magnetoelastic behaviour for samples with thicknesses between 1.3 and 90 nm.

Acknowledgments

This work was partially financed by the Spanish CICYT, under project code MAT98-0404.

We would like to thank Professor Carlos Otero of the Centro de Microscopía Electrónica 'Luis Bru' of the Complutense University of Madrid for the electron microscopy analysis.

References

[1] Miller J C 1994 *Laser Ablation* (*Springer Series in Material Science* vol 28) ed J C Miller (Berlin: Springer)
[2] Chrisey D B and Hubler G K (ed) 1994 *Pulsed Laser Deposition of Thin Films* (New York: Wiley)
[3] Singh R K, Lowndes D H, Chrisey D B, Forgarassy E and Narayan J (ed) 1998 *Advances in Laser Ablation of Materials* (*Mater. Res. Soc. Symp. Proc.* vol 526) (Pittsburg, PA: Materials Research Society)
[4] Hiroshima Y, Ishiguro T, Urata I, Ohta H, Tohogi M and Ichinose Y 1996 *J. Appl. Phys.* **79** 3572
[5] Nikitin P I, Beloglazov A, Yu A, Toporov M, Valeiko M V, Konov V Y, Perrone A, Luches A, Mirenghi L and Tapfer L 1997 *J. Appl. Phys.* **82** 1408
[6] Hayes J P, Stone L A, Snelling H V, Jenner A G and Greenough R D 1997 *IEEE Trans. Magn.* **33** 3613
[7] Madurga V, Vergara J, Ortega R J, Landazábal I P and Favieres C 1999 *Advanced Hard and Soft Magnetic Materials, 1998* (*Mater. Res. Soc. Symp. Proc.* vol 577) ed M Coey *et al* (Pittsburg, PA: Materials Research Society) p 599
[8] Favieres C and Madurga V 2001 *J. Non-Cryst. Solids* **287** 390
[9] Madurga V, Vergara J and Favieres C 2001 *Application of Ferromagnetic and Optical Materials, Storage and Magnetoelectronics* (*Mater. Res. Soc. Symp. Proc.* vol 674) ed H J Borg *et al* (Pittsburg, PA: Materials Research Society) p T.3.2.1
[10] Vergara J and Madurga V 2002 *J. Mater. Res.* **17** 2099
[11] Madurga V, Vergara J and Favieres C 2003 *J. Magn. Magn. Mater.* **254/255** 140
[12] Madurga V, Vergara J and Favieres C 2004 *J. Magn. Magn. Mater.* **272–276** 1681
[13] Bennet M R and Wright G J 1972 *Phys. Lett.* **6** 419
[14] Kwan M M L and Hoffman R W 1974 *Japan. J. Appl. Phys.* 1 **2** (Suppl.) 279
[15] Nikitan L V, Morinova L S, Litvintsev V V and Katkevich V N 1991 *Phys. Met. Metallogr.* **2** 92
[16] Pergolini S and Valdrè G 1997 *Nanostruct. Mater.* **9** 627
[17] Wiedemann G 1883 *Lebre von der Elektizitat* **3** 680
[18] Madurga V, Hernando A and Vázquez M 1981 *J. Phys. D: Appl. Phys.* **14** 913
[19] Madurga V, Hernando A and Nielsen O V 1984 *J. Phys. E: Sci. Instrum.* **17** 813
[20] Hernando A, Madurga V, Nuñez de Villavicencio C and Vázquez M 1984 *Appl. Phys. Lett.* **45** 802
[21] Favieres C, Aroca C, Sánchez M C, Rao K V and Madurga V 1999 *J. Magn. Magn. Mater.* **196/197** 224
[22] Hernando A, Vázquez M, Madurga V and Becerril J 1977 *IEEE Trans. Magn.* **13** 1511
[23] Favieres C, Aroca C, Sánchez M C and Madurga V 2000 *J. Appl. Phys.* **91** 9995
[24] Ercuta A, Mihalca I and Schlett Z 2002 *J. Appl. Phys.* **91** 9969
[25] Foltyn S R, Dye R C, Ott K C, Peterson E, Hubbard K M, Hutchinson W, Muenchausen R E, Estler R C and Wu X D 1991 *Appl. Phys. Lett.* **59** 594
[26] Landau L D and Lifshitz E M 1969 *Theory of Elasticity* (Barcelona: Reverté) p 101
[27] Favieres C and Madurga V 2004 *J. Appl. Phys.* at press
[28] Polack Ch, Knobel M, Grössinger R and Sato Turtelli R 1994 *J. Magn. Magn. Mater.* **134** 1